


Fission dynamics and entrance-channel study in the ^{210}Po compound nucleus via light-particle multiplicities

Chetan Sharma ^{*}, B. R. Behera , Shruti, Amit, Bharti Rohila , Amninderjeet Kaur, Subodh, Neha Dhanda , and Ashok Kumar[†]

Department of Physics, Panjab University, Chandigarh 160014, India

P. Sugathan, A. Jhingan, K. S. Golda, N. Saneesh, Mohit Kumar, H. Arora , and Divya Arora
Inter University Accelerator Centre, Aruna Asif Ali Marg, New Delhi 110067, India

H. P. Sharma 

Department of Physics, Banaras Hindu University, Varanasi, Uttar Pradesh 221005, India



(Received 2 May 2023; accepted 9 June 2023; published 28 June 2023)

Neutron multiplicities, folding angle distribution, mass distribution, and mass-energy distribution are measured for the compound nucleus ^{210}Po populated through the $^{12}\text{C} + ^{198}\text{Pt}$ reaction at an excitation energy of 61.6 MeV. The measured neutron multiplicities are compared with the statistical model code JOANNE2 to extract total fission time for the ^{210}Po compound nucleus. The total fission time (τ_{tot}) obtained for this system is $(10 \pm 5) \times 10^{-21}$ s at 49 MeV and increases to $(23 \pm 5) \times 10^{-21}$ at 61.8 MeV excitation energy indicating that dissipation increases with excitation energy. A comparison with τ_{tot} of the $^{18}\text{O} + ^{192}\text{Os}$ reaction populating the same compound nucleus indicates the influence of entrance channel mass asymmetry on the fission time. Dynamical model calculations have been performed to understand the fusion dynamics for these reactions and it is observed that the formation time of the compound nucleus increases as we go from the asymmetric to the symmetric entrance channels. Also, these calculations predict that 93% of the total angular momentum lead to the formation of a fully equilibrated compound nucleus for the $^{12}\text{C} + ^{198}\text{Pt}$ reaction whereas this percentage decreases to 84%, for the $^{18}\text{O} + ^{192}\text{Os}$ reaction indicating a higher percentage of noncompound nuclear processes in the latter case.

DOI: [10.1103/PhysRevC.107.064615](https://doi.org/10.1103/PhysRevC.107.064615)

I. INTRODUCTION

A heavy ion induced fission reactions mechanism has been studied for the past few decades to investigate the time scale of fusion and fission reactions [1–7], the existence of quasi-fission [8–11], and limits to the statistical model at high temperature and angular momentum [7,12]. It is now established that the process of fission is hindered due to the viscous nature of the compound nucleus (CN). This dissipative nature of CN enhances the emission of light particles (neutrons, protons, and α particles) that cannot be explained by standard statistical model of fission. The light particles emitted carry valuable information about the evolution of CN from its formation phase till its fission to two fully accelerated fragments. The multiplicity of these particles can be used as a clock to measure the lifetime of the composite nucleus prior to fission. For this, the number of neutrons emitted before and after fission are measured. In the conventional method, two sources of neutrons are observed in prompt coincidence with fission fragments. Neutrons emitted from the fused system moving with the CN velocity are referred as

pre-scission neutron multiplicity (ν_{pre}) and neutrons emitted from the fully accelerated fission fragments are named as post-scission neutron multiplicity (ν_{post}). Neutron evaporation also takes place from the dinuclear system before it attains the equilibrium configuration which also contributes to the pre-scission neutron multiplicity. These two contributions can be separated by taking into account the fact that the intensity of neutrons emitted from the fission fragments is strongly correlated with the direction of fission fragments whereas the neutrons emitted from the relatively slow moving compound system are weakly correlated with the beam direction. This angular correlations lead to the values of ν_{pre} and ν_{post} . The experimental values of ν_{pre} can be used to extract dissipation strength and fission time of the reaction by reproducing the ν_{pre} values in statistical model codes.

Charged particles multiplicity is another efficient probe to understand fusion-fission reaction dynamics [13–18]. This is because the energies and emission probabilities of charged particles are dependent on the shape of the emission source and this gives information of the deformation. But certain challenges are associated with charged particles measurements due to their low multiplicities.

Further, mass energy distribution of fission fragments is helpful in understanding the nature of competition between the process of fusion-fission and other noncompound nuclear

^{*}chetan1994s@gmail.com

[†]ashok@pu.ac.in

processes [clubbed together as quasifission (QF)] [19–21]. In QF, the entrance channel mass asymmetry remains preserved but it involves large dissipation of kinetic energy and angular momentum [22]. The presence of QF reduces the fusion cross section by preventing the fusion of heavy nuclei. It has been observed that the ratio of QF to fusion-fission is influenced by the entrance channel properties like the entrance channel mass asymmetry ($\alpha = \frac{A_1 - A_2}{A_1 + A_2}$) and charge product (Z_1, Z_2), where A_1, A_2 are mass numbers and Z_1, Z_2 are atomic numbers of the target and projectile, respectively [23–25]. Studies like mass distribution (MD), mass-energy distribution (MED), and mass-angle distribution (MAD) of fission fragments are some of the experimental probes to understand the competition of QF and fusion-fission. It becomes essential to separate the QF contribution from true fusion-fission events when we are studying the fusion-fission reaction dynamics.

With this motivation, the present work aims to measure the pre-scission neutron multiplicity ν_{pre} for ^{210}Po CN populated through the reaction $^{12}\text{C} + ^{198}\text{Pt}$ at 81 MeV energy. Total fission time has been extracted using these ν_{pre} values by incorporating delays in statistical model code JOANNE2. Dynamical model calculations are also carried out to estimate the formation time for the reaction under study. These dynamical model calculations are also done for the $^{18}\text{O} + ^{192}\text{Os}$ reaction which populates the same CN ^{210}Po . Mass distribution and mass energy distribution for the same reaction have also been done to disentangle noncompound nuclear processes from the true fusion-fission. The findings are discussed in later sections.

This paper is organized in the following manner. The experimental setup is described in Sec. II and Sec. III involves data analysis techniques for fission fragments and neutron multiplicity. Section IV describes the theoretical calculations involving statistical and dynamical models and their discussion, followed by the results of analysis summarized and concluded in Sec. V.

II. EXPERIMENTAL SETUP

The experiment aiming to measure neutron multiplicity was carried out using the National Array of Neutron Detectors (NAND) facility at IUAC, New Delhi. ^{12}C beam at 81 MeV energy was bombarded on 2.1 mg/cm² thick ^{198}Pt target to populate the ^{210}Po CN at an excitation energy of 61.6 MeV. The ion beam has the repetition rate of 250 ns and intensity of ~ 0.9 pA. Two 20 cm \times 10 cm position sensitive multiwire proportional counters (MWPCs) were placed at folding angles to detect fission fragments. These MWPCs were operated with isobutane gas at a pressure of 4 torr. 16 BC501A liquid scintillators placed in the reaction plane of the NAND array were used to detect neutrons. These detectors have an active area of 5 in. \times 5 in. and are coupled to a 5 in. photomultiplier tube (PMT Model Hamamatsu R4144). The data acquisition system was triggered by the logic OR of time of flight (TOF) signal from both MWPCs logically ANDed with the radiofrequency (RF) of the beam to avoid false triggering. The whole systematic of experimental setup is shown in Fig. 1. To separate neutrons from γ s, the neutron- γ discrimination was done using

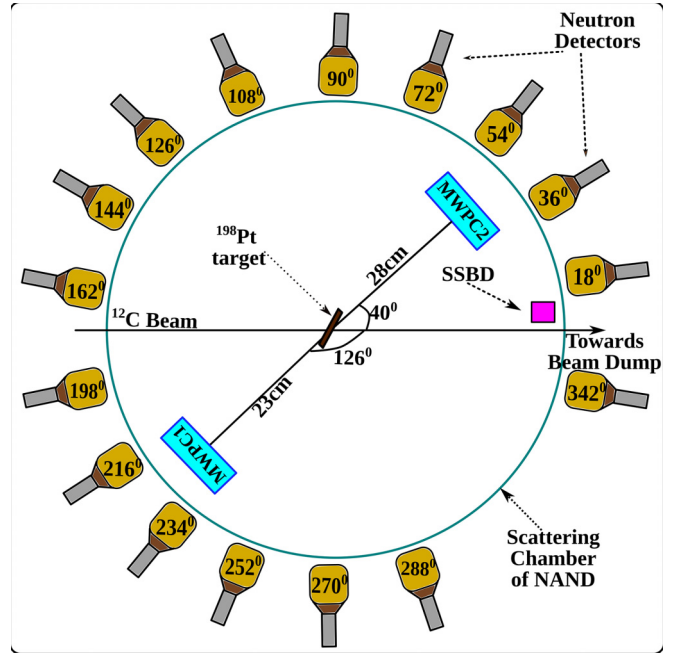


FIG. 1. Detectors arrangement during the experiment.

the zero-crossing technique. Figure 2 shows the pulse shape discrimination (PSD) spectrum from the neutron detector having well-separated neutron events. Fission events were selected from the time correlation of two MWPCs shown in Fig. 3. The calibration of all time to digital converters was performed using the data from OTREC time calibrator module which gives pulses of fixed time interval. The data in the event mode were collected using the ROOT based data acquisition system. In order to prevent any contamination in the data, the beam was dumped 4.5 m away from the target and was properly shielded with borated paraffin blocks and lead sheets.

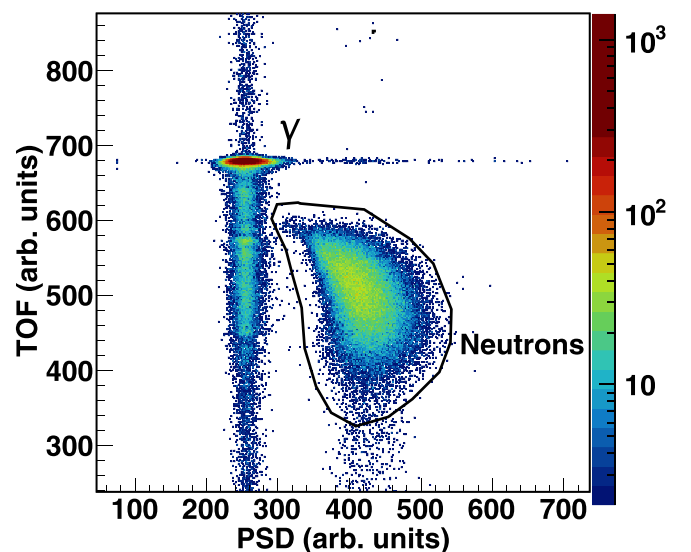


FIG. 2. PSD vs TOF from one of the neutron detectors.

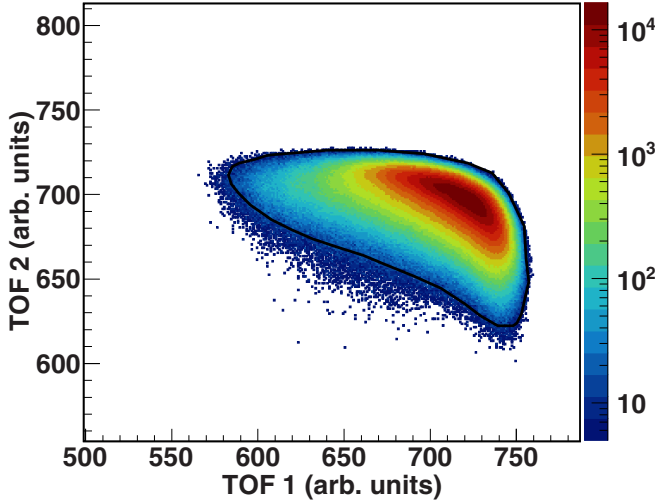


FIG. 3. Time correlation of both MWPCs. Solid black line is the fission gate.

III. DATA ANALYSIS AND RESULTS

The objective of the experiment was to measure neutron multiplicities, mass ratio distribution, and mass energy distribution of the fission fragments for the $^{12}\text{C} + ^{198}\text{Pt}$ reaction and interpret the results using theoretical calculations. The detailed steps involved in the data analysis are given in the following subsections.

A. Mass energy distribution of fission fragments

The position calibration of MWPCs was done using the known positions of edges of the illuminated area of the MWPC detectors used during the experiment. The calibrated positions, both X and Y , were converted event by event to polar θ and azimuthal ϕ angles using standard kinematics. Finally, a folding angle distribution is obtained by adding θ_1 and θ_2 from both MWPCs. Figure 4(a) shows the scatter plot of θ_{fold} versus ϕ_{fold} . The most intense region corresponds to the folding angle of 166.5° and $\phi_{1\text{lab}} + \phi_{2\text{lab}} = 180^\circ$. The velocity of the fission fragments was determined using the absolute time method (ATM) [26]. In this method, velocity vectors of fission fragments were determined from the position and individual TOF information from both MWPCs.

The velocity of the fissioning system in laboratory frame (\vec{v}_{lab}) can be split into two orthogonal components which are parallel (\vec{v}_{par}) and perpendicular (\vec{v}_{perp}) to the beam axis. These components can be expressed in measurable quantities (angles and velocity of fission fragments) [26] as

$$\vec{v}_{\text{par}} = \frac{v_{1\text{lab}}v_{2\text{lab}} \sin(\theta_{1\text{lab}} + \theta_{2\text{lab}})}{v_{1\text{lab}} \sin \theta_{1\text{lab}} + v_{2\text{lab}} \sin \theta_{2\text{lab}}} \quad (1)$$

and

$$\vec{v}_{\text{perp}} = \frac{v_{1\text{lab}}v_{2\text{lab}} \sin \theta_{1\text{lab}} \sin \theta_{2\text{lab}} \sin \phi_{12\text{lab}}}{V^{1/2}}, \quad (2)$$

where $\phi_{12\text{lab}}$ is the azimuthal folding angle and $\theta_{1\text{lab}}$ and $\theta_{2\text{lab}}$ are the scattering angles of the fission fragments 1 and 2,

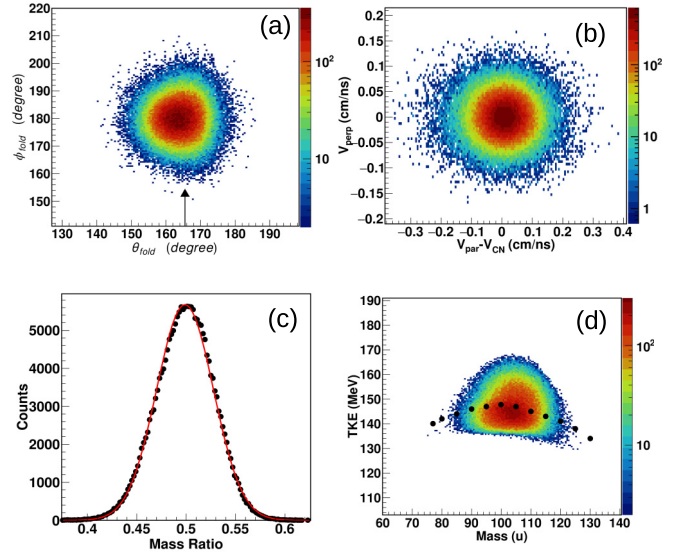


FIG. 4. (a) Scatter plot of folding angle distribution. Arrow corresponds to θ_{fold} calculated considering full momentum transfer (165.5°), (b) velocity distribution, (c) mass ratio distribution, and (d) mass energy distribution. Dotted points indicate TKE calculated using Viola systematics.

respectively. The quantity V is given by

$$V = v_{1\text{lab}}^2 \sin^2 \theta_{1\text{lab}} + v_{2\text{lab}}^2 \sin^2 \theta_{2\text{lab}} - 2v_{1\text{lab}}v_{2\text{lab}} \sin \theta_{1\text{lab}} \sin \theta_{2\text{lab}} \cos \phi_{12\text{lab}}. \quad (3)$$

The experimentally measured velocities were corrected in an iterative way explained in Ref. [27] until the correction did not further change the velocity significantly. Figure 4(b) shows the scatter plot of $(v_{\text{par}} - v_{\text{CN}})$ versus v_{perp} . For full momentum transfer fission events, v_{par} is expected to match the velocity of CN in laboratory frame (v_{CN}). The mass ratio of fission fragments was deduced from the conservation of linear momentum ($m_1 \vec{v}_{1\text{c.m.}} = m_2 \vec{v}_{2\text{c.m.}}$) by using the relation

$$M_r = \frac{m_1}{m_1 + m_2} = \frac{v_{2\text{c.m.}}}{v_{1\text{c.m.}} + v_{2\text{c.m.}}}. \quad (4)$$

The mass ratio distribution [Fig. 4(c)] has a single Gaussian peak which reveals that fission is taking place only from the CN. No signature of noncompound nucleus fission (NCNF) has been observed for this system at 61.6 MeV excitation energy. The standard deviation of mass ratio distribution (σ_{MR}) was found to be 0.028 which is lower than the upper limit (0.07) for the fission followed by complete fusion [28].

The center of mass total kinetic energy (TKE) of fission fragments was obtained from the measured masses and velocities of the fission fragments. The two-dimensional (2D) scatter plot of mass and TKE is shown in Fig. 4(d) comprising of only fusion-fission events. A comparison with Viola systematics [29] (indicated by black dotted points) shows good agreement and indicates the parabolic dependence of TKE on the fission fragment masses. From these observations we may, therefore, conclude that the reaction under study is dominated by full momentum transfer followed by binary fission and that

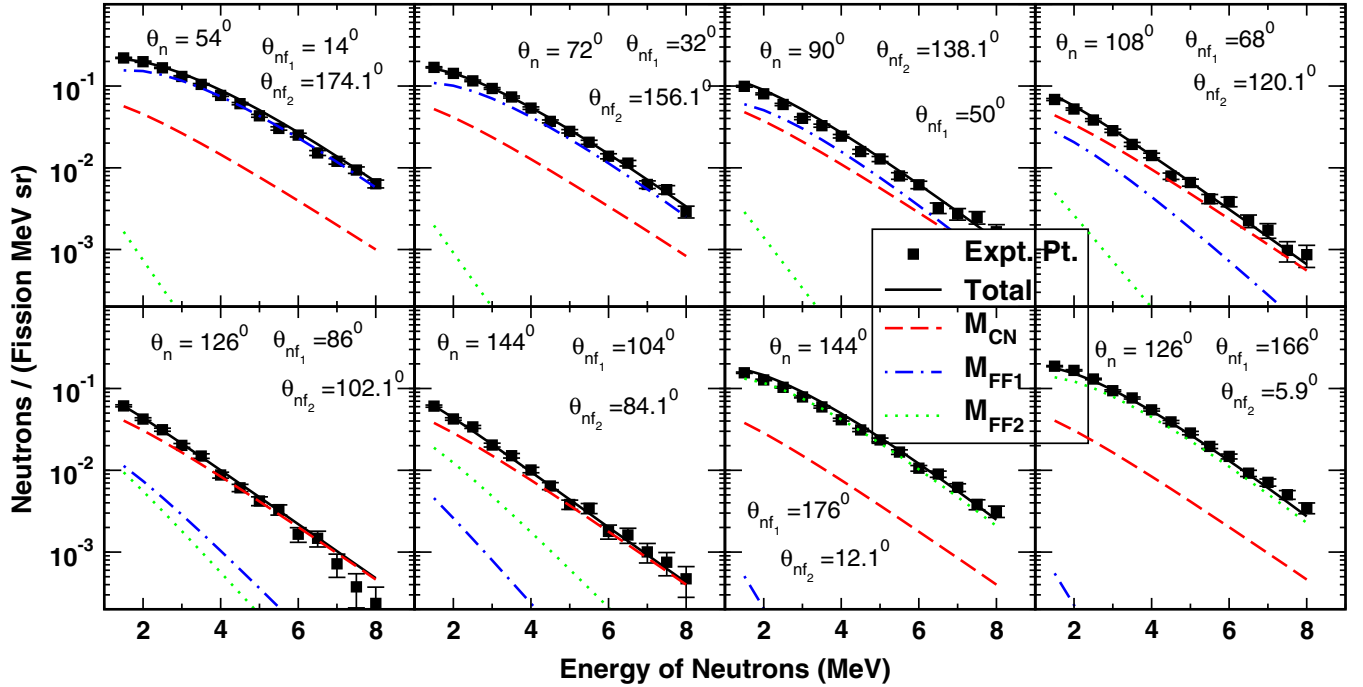


FIG. 5. Neutron multiplicity spectra for $^{12}\text{C} + ^{198}\text{Pt}$ system at an excitation energy of 61.6 MeV. Solid squares represent experimental data points. The fit for the pre-scission (red dashed line) and post-scission contribution from one fragment (blue dashed dotted line) and other fragment (green dotted line) are also shown. The solid black line represents the sum of all the three contributions. θ_n is the neutron detector angle with respect to beam axis. θ_{nf_1} and θ_{nf_2} are relative angles between neutrons emitted and the fission fragments.

the transfer induced fission is insignificant in this reaction at the given excitation energy.

B. Neutron multiplicity

The TOF spectra obtained from neutron detectors were gated with fission and neutrons to obtain true neutron events. These gated spectra were calibrated using a precision time to amplitude converter calibrator data and the prompt γ -ray peak as reference and converted to neutron energy spectra using the relation

$$E_n = \frac{1}{2} M_n \left(\frac{l}{t} \right)^2, \quad (5)$$

where M_n is mass of neutron, l is neutron flight path from target to detector (175 cm), and t is the TOF of neutrons. The final neutron energy spectra obtained were corrected with energy dependent neutron detection efficiency. These energy spectra can have contributions from three sources: (i) compound nucleus as pre-scission multiplicity (M_{pre}), (ii) fission fragment as post-scission multiplicity (M_{post}), and (iii) complementary fission fragment as post-scission multiplicity (M_{post}). So, the total neutron multiplicity is given by

$$M_{\text{tot}} = M_{\text{pre}} + 2 \times M_{\text{post}}. \quad (6)$$

The contribution from noncompound nuclear processes is ignored since its contribution is almost negligible for the system under study. Considering these three emission sources, the neutron energy spectra were fitted simultaneously with the

Watt expression [30] given by

$$\frac{d^2 M}{dE_n d\Omega} = \sum_{i=1}^3 \frac{M_i \sqrt{E_n}}{2(\pi T_i)^{3/2}} \times \exp \left[-\frac{E_n - 2\sqrt{E_n E_i / A_i} \cos \theta_i + E_i / A_i}{T_i} \right], \quad (7)$$

where E_n is the neutrons energy in laboratory frame, A_i , E_i , and T_i are the mass, energy, and temperature of each neutron emitting source. M_i is the multiplicity for each contribution. θ_i is the emission angle of neutron with respect to its emitting source. T_{pre} was calculated using the relation

$$T_{\text{pre}} = \sqrt{\frac{E^*}{a}}, \quad (8)$$

where E^* is the excitation energy of CN and a is the level density parameter. The value of a is assumed to be $A_{\text{CN}}/10 \text{ MeV}^{-1}$ and is further scaled down by the factor of 11/12 to account for the cascade of sequential particle evaporation [31]. All the neutron energy spectra were fitted simultaneously keeping M_{pre} , M_{post} , T_{pre} , and T_{post} as free parameters and also by keeping the temperatures fixed. The values of these free parameters obtained after fitting are $M_{\text{pre}} = 2.06 \pm 0.05$, $M_{\text{post}} = 1.22 \pm 0.01$, $T_{\text{pre}} = 1.25 \pm 0.02$, and $T_{\text{post}} = 0.91 \pm 0.01$. The fitted plots are shown in Fig. 5. The M_{pre} values obtained were compared with the results of Ref. [32] and were found to be in agreement with the previously published data.

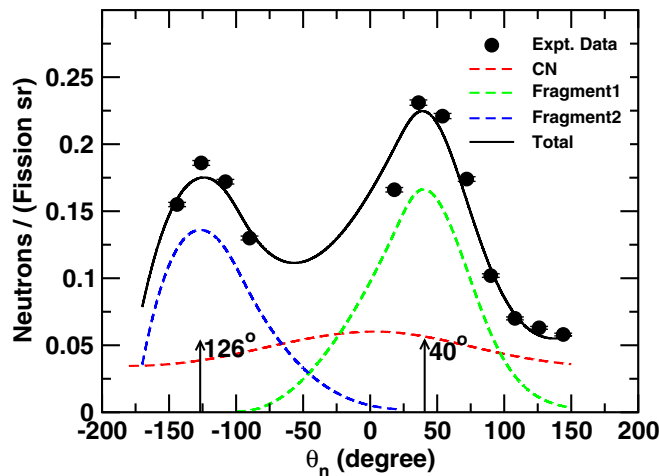


FIG. 6. Neutron angular distribution along with multiple-source fitting (solid lines). The dashed red line corresponds to the pre-scission contribution while blue and green dashed lines correspond to the individual post-scission contributions from fragment1 and fragment2.

A typical angular distribution of neutron multiplicity spectrum is shown in Fig. 6. The angular distribution from all three emitting sources has a Gaussian distribution. The contribution from fission fragments peaks around the angle where fission detectors were placed. The contribution from CN peaks around the beam direction. Both these observations confirm that there are strong angular correlations of neutrons emitted from these sources due to the kinematic focusing effects. This strong angular correlation of neutrons emitted from fission fragments serve as the basis for the separation of pre-scission neutrons from the post-scission neutrons.

IV. STATISTICAL MODEL CALCULATIONS

In order to understand the strength of dissipation in fusion-fission process, statistical model calculations were done using the JOANNE2 code [33,34]. JOANNE2 is a Monte Carlo simulation code which calculates fission time by taking into account the effects of deformation on particle binding energies and transmission coefficients. Deformation dependent level density parameters are calculated within the code for both spherical and deformed nucleus using the Toke and Swiatecki formalism [35]. The a_f/a_v ratio and diffuseness parameter are also adjustable parameters in the code. The transmission coefficients used in the code are derived from the universal optical parameters [36,37]. Fission barriers are calculated using the rotating finite range model (RFRM) without a scaling factor [38]. The deformation energy and rotational energy at the equilibrium and saddle-point are also taken from RFRM.

The decay modes chosen by the JOANNE2 code are fission, neutron, proton, and α evaporation. However, the dominant process of cooling in heavy ion fusion-fission reactions is by evaporation of neutrons. The two contributions in the fission time, viz. transient time (τ_{tr}) and saddle-to-scission time (τ_{ssc}), can be extracted from experimentally measured neutron multiplicities using the JOANNE2 code to understand the strength of dissipation in heavy ion induced fusion-fission

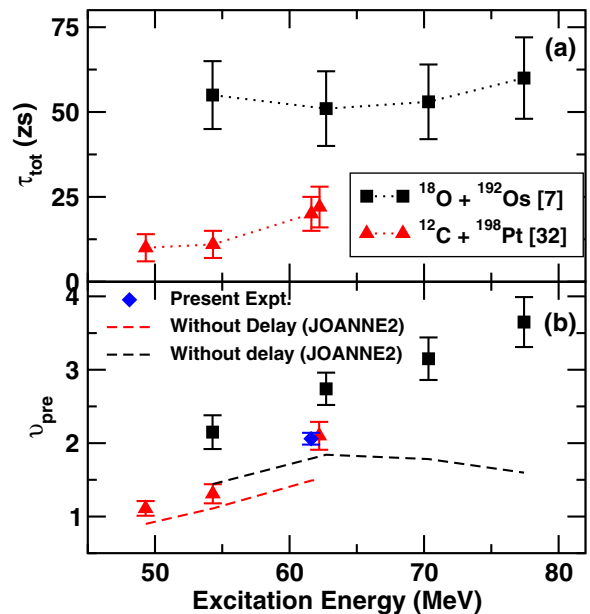


FIG. 7. (b) Experimental neutron multiplicity for $^{12}\text{C} + ^{198}\text{Pt}$ and $^{18}\text{O} + ^{192}\text{Os}$ reactions at different excitation energies. ν_{pre} values for $^{18}\text{O} + ^{192}\text{Os}$ are taken from Ref. [7]. Dashed lines in (b) are the ν_{pre} values calculated without incorporating delay in JOANNE2 (a) τ_{tot} (calculated using JOANNE2) required to reproduce the experimental ν_{pre} values.

reactions. In this code, the whole fission path is divided into two parts: mean pre-saddle deformation Z_{tr} and mean saddle-to-scission deformation Z_{ssc} , where Z is the elongation of symmetric axis in units of the diameter of the spherical nucleus. Both τ_{tr} and τ_{ssc} can be varied in this code to reproduce the experimentally measured neutron multiplicities at fixed deformation value. Saxena *et al.* [39] and several other authors have quoted the value of τ_{tr} to be about $(5-10) \times 10^{-21}$ s. We have done our calculations at fixed value of $\tau_{tr} = 10 \times 10^{-21}$ s and varied τ_{ssc} to reproduce experimentally measured neutron multiplicities. Figures 7(a) and 7(b) represent the total fission time (τ_{tot}) and pre-scission neutron multiplicity (ν_{pre}), respectively, as a function of excitation energy for the reactions $^{12}\text{C} + ^{198}\text{Pt}$ and $^{18}\text{O} + ^{192}\text{Os}$ populating the same CN ^{210}Po . The difference in ν_{pre} values for the two reactions is due to the entrance channel effects [39–41]. Red and black dashed lines in Figure 7(b) are the ν_{pre} for reactions $^{12}\text{C} + ^{198}\text{Pt}$ and $^{18}\text{O} + ^{192}\text{Os}$, respectively, calculated using JOANNE2 without including delays. Clearly, a total fission time of $(10-23) \pm 5 \times 10^{-21}$ s is required to reproduce the experimental ν_{pre} values for $^{12}\text{C} + ^{198}\text{Pt}$ reaction whereas $\tau_{tot} = (50-60) \pm 10 \times 10^{-21}$ s reproduce ν_{pre} values for the $^{18}\text{O} + ^{192}\text{Os}$ reaction. The difference in total fission time can be inferred as the time required by the dinuclear system to fully equilibrate to CN which is different for these two reactions. This delay time is known as the formation time of CN (τ_{fo}) and it depends on the entrance channel chosen to populate the CN. So, the information of τ_{fo} becomes important to fully understand the fission-fission process. The dynamical approach can be applied to study the fusion dynamics and formation time of the CN which is explained in the following section.

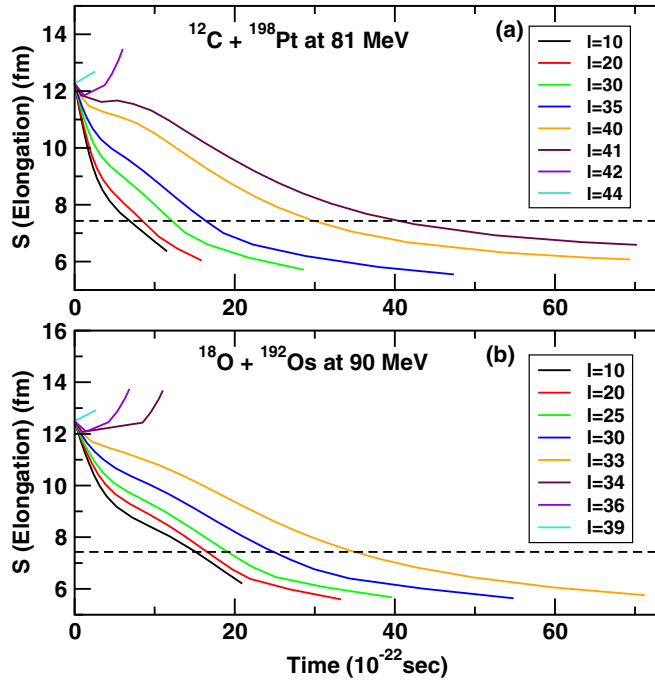


FIG. 8. Calculated time evolution of the separation (S) of the colliding nuclei as a function of time at various l values for the reactions (a) $^{12}\text{C} + ^{198}\text{Pt}$ at 81 MeV and (b) $^{18}\text{O} + ^{192}\text{Os}$ at 90 MeV. Dashed line in both the figures corresponds to the radius $R = R_0 A^{1/3}$ for the compound nucleus ^{210}Po .

V. HICOL CALCULATIONS

Dynamical model calculations were performed for the $^{12}\text{C} + ^{198}\text{Pt}$ system at 61.6 MeV excitation energy using the HICOL code. In this model, developed by Feldmeier [42], the dynamical evolution of the two colliding nuclei is described by a series of shapes which consist of two spheres connected by a conical neck. Throughout the collision process, the volume of the shape is conserved to maintain uniform mass and charge densities. These shapes are determined by a set of three macroscopic degrees of freedom which are unique for each shape. These are elongation (s), the neck-coordinate (σ), and the asymmetric coordinate (δ), defined as follows:

$$s = \text{distance between the two colliding spheres}, \quad (9)$$

$$\sigma = \frac{V_0 - \left(\frac{4\pi}{3}R_1^3\right) - \left(\frac{4\pi}{3}R_2^3\right)}{V_0}, \quad (10)$$

$$\Delta = \frac{R_1 - R_2}{R_1 + R_2}, \quad (11)$$

where V_0 is the total volume of the system and is independent of s , σ , and Δ . R_1 and R_2 are the radii of the two colliding nuclei. This model gives a realistic macroscopic description of the nucleus-nucleus collision, based on the concept of one-body dissipation which means that the dissipation arises due to the collision of independent particles with the moving walls of the nucleus [43]. The results of HICOL calculations are given in Figs. 8 and 9. Figure 8 represents the elongation (s) of the fusing nuclei as a function of time at various l values. Calculations are also done for $^{18}\text{O} + ^{192}\text{Os}$ for

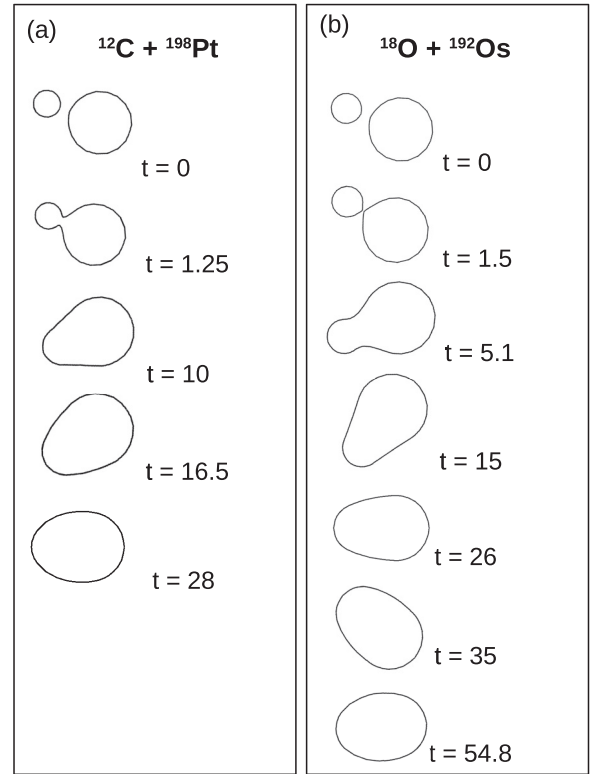


FIG. 9. Time evolution of the reactions (a) $^{12}\text{C} + ^{198}\text{Pt}$ and (b) $^{18}\text{O} + ^{192}\text{Os}$ for an angular momentum of $30\hbar$

comparison which populates the same CN ^{210}Po . From Fig. 8(a), it is observed that, for angular momenta $l > 41\hbar$, the two nuclei are separated quickly before being fused together (the case of deep inelastic collision). For low angular momenta, the trajectories remained elongated for long times with decreasing separation between the colliding nuclei (the case of fusion). The dashed lines in Fig. 8 shows the radius of the CN ^{210}Po calculated using the relation $R = R_0 A^{1/3}$. In the case of $^{12}\text{C} + ^{198}\text{Pt}$, the HICOL predicts fusion to occur for $l < 41\hbar$ and in the case of $^{18}\text{O} + ^{192}\text{Os}$, it predicts fusion for $l < 30\hbar$ only. Figure 9 represents the time evolution of shapes for the ^{210}Po nucleus populated through two different channels $^{12}\text{C} + ^{198}\text{Pt}$ and $^{18}\text{O} + ^{192}\text{Os}$ at $l = 30\hbar$. It is found that the formation time for the $^{12}\text{C} + ^{198}\text{Pt}$ system is much less than the formation time for the $^{18}\text{O} + ^{192}\text{Os}$ system. So, there is a gradual increase in the formation time of CN as one goes from the asymmetric to the symmetric system in the entrance channel. Considering that the emission of neutrons also takes place from the dinuclear system before it attains the equilibrium configuration, the number of neutrons emitted during the τ_{fo} of $^{18}\text{O} + ^{192}\text{Os}$ will be more due to its larger formation time than the $^{12}\text{C} + ^{198}\text{Pt}$ reaction. These observations suggest that the observed pre-scission neutron multiplicity and fission delay for $^{12}\text{C} + ^{198}\text{Pt}$ and $^{18}\text{O} + ^{192}\text{Os}$ reactions can be understood quantitatively if we consider different τ_{fo} values as predicted by dynamical code HICOL.

VI. SUMMARY AND CONCLUSION

In the present study, fusion-fission reaction dynamics of ^{210}Po CN has been investigated using neutron multiplicity as

a probe. From the mass ratio distribution, symmetric fission is observed with negligible contribution from noncompound nuclear fission processes. Fission time calculated through statistical model code JOANNE2 for the two reactions $^{12}\text{C} + ^{198}\text{Pt}$ and $^{18}\text{O} + ^{192}\text{Os}$ indicates the presence of a dissipative nature which increases with excitation energy. A comparison of τ_{tot} for these reaction indicates the presence of entrance channel effects which influences the fusion-fission dynamics. Dynamical model calculations through HICOL for $^{12}\text{C} + ^{198}\text{Pt}$ and $^{18}\text{O} + ^{192}\text{Os}$ reactions predict that the formation time of CN is different for these two reactions. To explain the difference in pre-scission neutron multiplicity values and fission time for the two reactions under study, both statistical and

dynamical approaches are required. Also it is found that, for the $^{12}\text{C} + ^{198}\text{Pt}$ reaction, fusion occurs for l values less than $41\hbar$ and in the case of $^{18}\text{O} + ^{192}\text{Os}$, fusion occurs for l values less than $30\hbar$.

ACKNOWLEDGMENTS

The authors would like to acknowledge the Pelletron group at IUAC for a smooth running of the accelerator during the experiment. The authors want to thank Target Laboratory, IUAC for providing an isotopically enriched ^{198}Pt target. One of the authors C.S. wants to thank J. P. Lestone for providing the JOANNE2 code.

-
- [1] D. J. Hinde, D. Hilscher, H. Rossner, B. Gebauer, M. Lehmann, and M. Wilpert, *Phys. Rev. C* **45**, 1229 (1992).
- [2] A. Gavron, A. Gayer, J. Boissevain, H. C. Britt, J. R. Nix, A. J. Sierk, P. Grange, S. Hassani, H. A. Weidenmiller, J. R. Beene, B. Cheynis, D. Drain, R. L. Ferguson, F. E. Obenshain, F. Plasil, G. R. Young, G. A. Pettitt, and C. Butler, *Phys. Lett. B* **176**, 312 (1986).
- [3] H. Rossner, D. Hilscher, D. J. Hinde, B. Gebauer, M. Lehmann, M. Wilpert, and E. Mordhorst, *Phys. Rev. C* **40**, 2629 (1989).
- [4] J. P. Lestone, J. R. Leigh, J. O. Newton, D. J. Hinde, J. X. Wei, J. X. Chen, S. Elfstrom, and D. G. Popescu, *Phys. Rev. Lett.* **67**, 1078 (1991).
- [5] K. Kapoor, S. Verma, P. Sharma, R. Mahajan, N. Kaur, G. Kaur, B. R. Behera, K. P. Singh, A. Kumar, H. Singh, R. Dubey, N. Saneesh, A. Jhingan, P. Sugathan, G. Mohanto, B. K. Nayak, A. Saxena, H. P. Sharma, S. K. Chamoli, I. Mukul, and V. Singh, *Phys. Rev. C* **96**, 054605 (2017).
- [6] C. Sharma, K. Kapoor, and A. Kumar, *Eur. Phys. J. A* **59**, 10 (2023).
- [7] J. O. Newton, D. J. Hinde, R. J. Charity, J. R. Leigh, J. J. M. Bokhorst, A. Chatterjee, G. S. Foote, and S. Ogaza, *Nucl. Phys. A* **483**, 126 (1988).
- [8] E. Prasad, K. M. Varier, R. G. Thomas, P. Sugathan, A. Jhingan, N. Madhavan, B. R. S. Babu, Rohit Sandal, Sunil Kalkal, S. Appannababu, J. Gehlot, K. S. Golda, S. Nath, A. M. Vinodkumar, B. P. Ajith Kumar, B. V. John, Gayatri Mohanto, M. M. Musthafa, R. Singh, A. K. Sinha, and S. Kailas, *Phys. Rev. C* **81**, 054608 (2010).
- [9] R. du Rietz, E. Williams, D. J. Hinde, M. Dasgupta, M. Evers, C. J. Lin, D. H. Luong, C. Simenel, and A. Wakhle, *Phys. Rev. C* **88**, 034611 (2013).
- [10] Kavita, K. S. Golda, T. K. Ghosh, A. Jhingan, P. Sugathan, A. Chatterjee, B. R. Behera, A. Kumar, R. Kumar, N. Saneesh, M. Kumar, A. Yadav, C. Yadav, N. Kumar, A. Banerjee, A. Rani, S. K. Duggi, R. Dubey, K. Rani, S. Noor, J. Acharya, and H. Singh, *Phys. Rev. C* **100**, 024626 (2019).
- [11] S. Gupta, C. Schmitt, K. Mahata, A. Shrivastava, P. Sugathan, A. Jhingan, K. S. Golda, N. Saneesh, M. Kumar, G. Kaur, L. Stuttgé, D. Arora, H. Arora, A. Chatterjee, K. Chauhan, S. K. Duggi, D. P. Kaur, V. Mishra, P. N. Patil, and K. Rani, *Phys. Rev. C* **100**, 064608 (2019).
- [12] W. P. Zank, D. Hilscher, G. Ingold, U. Jahnke, M. Lehmann, and H. Rossner, *Phys. Rev. C* **33**, 519 (1986).
- [13] A. Chatterjee, A. Navin, S. Kailas, P. Singh, D. C. Biswas, A. Karnik, and S. S. Kapoor, *Phys. Rev. C* **52**, 3167 (1995).
- [14] T. C. Awes, G. Poggi, C. K. Gelbke, B. B. Back, B. G. Glagola, H. Breuer, and V. E. Viola, *Phys. Rev. C* **24**, 89 (1981).
- [15] C. Y. Wong, *Phys. Rev. Lett.* **31**, 766 (1973).
- [16] Y. K. Gupta, D. C. Biswas, R. K. Choudhury, A. Saxena, B. K. Nayak, B. John, K. Ramachandran, R. G. Thomas, L. S. Danu, B. N. Joshi, K. Mahata, S. K. Pandit, and A. Chatterjee, *Phys. Rev. C* **84**, 031603(R) (2011).
- [17] R. Yanez, T. A. Bredeweg, E. Cornell, B. Davin, K. Kwiatkowski, V. E. Viola, R. T. de Souza, R. Lemmon, and R. Popescu, *Phys. Rev. Lett.* **82**, 3585 (1999).
- [18] H. Ikezoe, Y. Nagame, I. Nishinaka, Y. Sugiyama, Y. Tomita, K. Ideno, S. Hamada, N. Shikazono, A. Iwamoto, and T. Ohtsuki, *Phys. Rev. C* **49**, 968 (1994).
- [19] W. J. Swiatecki, *Phys. Scr.* **24**, 113 (1981).
- [20] S. Bjornholm and W. J. Swiatecki, *Nucl. Phys. A* **391**, 471 (1982).
- [21] W. Q. Shen, J. Albinski, A. Gobbi, S. Gralla, K. D. Hildenbrand, N. Herrmann, J. Kuzminski, W. F. J. Müller, H. Stelzer, J. Tke, B. B. Back, S. Bjornholm, and S. P. Srensen, *Phys. Rev. C* **36**, 115 (1987).
- [22] J. P. Blocki, H. Feldmeier, and W. J. Swiatecki, *Nucl. Phys. A* **459**, 145 (1986).
- [23] D. J. Hinde, M. Dasgupta, and A. Mukherjee, *Phys. Rev. Lett.* **89**, 282701 (2002).
- [24] B. B. Back, P. B. Fernandez, B. G. Glagola, D. Henderson, S. Kaufman, J. G. Keller, S. J. Sanders, F. Videbaek, T. F. Wang, and B. D. Wilkins, *Phys. Rev. C* **53**, 1734 (1996).
- [25] R. Rafiei, R. G. Thomas, D. J. Hinde, M. Dasgupta, C. R. Morton, L. R. Gasques, M. L. Brown, and M. D. Rodriguez, *Phys. Rev. C* **77**, 024606 (2008).
- [26] D. J. Hinde, M. Dasgupta, J. R. Leigh, J. C. Mein, C. R. Morton, J. O. Newton, and H. Timmers, *Phys. Rev. C* **53**, 1290 (1996).
- [27] M. Thakur, B. R. Behera, R. Mahajan, N. Saneesh, G. Kaur, P. Sharma, R. Dubey, K. Kapoor, A. Yadav, N. Kumar *et al.*, *Eur. Phys. J. A* **53**, 133 (2017).
- [28] C. Simenel, D. J. Hinde, R. du Rietz, M. Dasgupta, M. Evers, C. J. Lin, D. H. Luong, and A. Wakhle, *Phys. Lett. B* **710**, 607 (2012).
- [29] V. E. Viola, K. Kwiatkowski, and M. Walker, *Phys. Rev. C* **31**, 1550 (1985).
- [30] D. Hilscher, J. R. Birkelund, A. D. Hoover, W. U. Schröder, W. W. Wilcke, J. R. Huizenga, A. C. Mignerey, K. L.

- Wolf, H. F. Breuer, and V. E. Viola, *Phys. Rev. C* **20**, 576 (1979).
- [31] E. Holub, D. Hilscher, G. Ingold, U. Jahnke, H. Orf, and H. Rossner, *Phys. Rev. C* **28**, 252 (1983).
- [32] K. S. Golda, A. Saxena, V. Mittal, K. Mahata, P. Sugathan, A. Jhingan, V. Singh, R. Sandal, S. Goyal, J. Gehlot, A. Dhal, B. Behera, R. Bhowmik, and S. Kailas, *Nucl. Phys. A* **913**, 157 (2013).
- [33] J. P. Lestone, *Phys. Rev. Lett.* **70**, 2245 (1993).
- [34] J. P. Lestone and S. G. McCalla, *Phys. Rev. C* **79**, 044611 (2009).
- [35] J. Toke and W. J. Swiatecki, *Nucl. Phys. A* **372**, 141 (1981).
- [36] J. R. Huizenga and G. Igo, *Nucl. Phys.* **29**, 462 (1962).
- [37] C. M. Perey and F. G. Perey, *At. Data Nucl. Data Tables* **17**, 1 (1976).
- [38] A. J. Sierk, *Phys. Rev. C* **33**, 2039 (1986).
- [39] A. Saxena, A. Chatterjee, R. K. Choudhary, S. S. Kapoor, and D. M. Nandkarni, *Phys. Rev. C* **49**, 932 (1994).
- [40] H. Singh, A. Kumar, B. R. Behera, I. M. Govil, K. S. Golda, P. Kumar, A. Jhingan, R. P. Singh, P. Sugathan, M. B. Chatterjee, S. K. Datta, Ranjeet, S. Pal, and G. Viesti, *Phys. Rev. C* **76**, 044610 (2007).
- [41] M. Shareef, A. Chatterjee, and E. Prasad, *Eur. Phys. J. A* **52**, 342 (2016).
- [42] H. Feldmeier, *Rep. Prog. Phys.* **50**, 915 (1987).
- [43] J. Blocki, R. Planeta, J. Brzychczyk, and K. Grotowski, *Z. Phys. A* **341**, 307 (1992).